The Functionalizing Effect of Increasingly Graphitic Carbon Supports on Carbon-Supported and TiO2–Carbon Composite-Supported Pt Nanoparticles

ARTICLE *in* THE JOURNAL OF PHYSICAL CHEMISTRY C · OCTOBER 2012

Impact Factor: 4.77 · DOI: 10.1021/jp304947y

4 AUTHORS, INCLUDING:

Jiwei Ma
Pierre and Marie Curie University - Paris 6
23 PUBLICATIONS **160** CITATIONS
SEE PROFILE

Aurelien Habrioux
Université de Poitiers
35 PUBLICATIONS **460** CITATIONS
SEE PROFILE

Nicolas Alonso-Vante
Université de Poitiers
226 PUBLICATIONS **4,592** CITATIONS
SEE PROFILE

THE JOURNAL OF PHYSICAL CHEMISTRY C

Article

pubs.acs.org/JPCC

Functionalizing Effect of Increasingly Graphitic Carbon Supports on Carbon-Supported and TiO_2–Carbon Composite-Supported Pt Nanoparticles

J. Ma, A. Habrioux, N. Guignard, and N. Alonso-Vante*

IC2MP, UMR-CNRS 7285, University of Poitiers, 4 rue Michel Brunet, 86022 Poitiers, France

Supporting Information

ABSTRACT: Strong interaction between Pt nanoparticles and graphitic carbon in carbon-based and oxide–carbon composite substrates is demonstrated using electrochemical CO stripping experiments. A correlation between the in-plane crystallite size of the carbon supports and the oxidation charge of CO stripping wave was made. It appears that π-system of graphitized carbon anchors platinum particles in a way that strongly modifies the electronic properties of the Pt valence band. The effects of graphitized carbon on platinum are even observable on TiO_2–carbon composite-supported Pt, where a well-known strong metal–support interaction between Pt and TiO_2 is already present, demonstrating the significant extent of the interaction between Pt and graphite. Finally, a preliminary proof of the role played by the interfacial Pt–Ti nanoalloy on oxide–carbon composite is given.

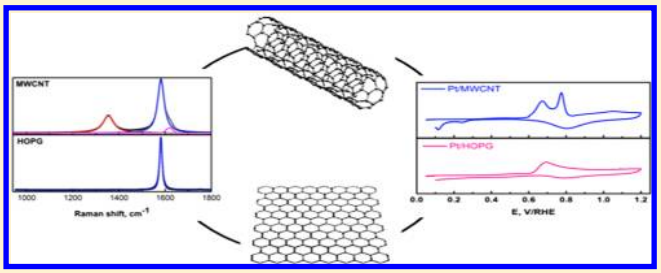

1. INTRODUCTION

The changes of electronic properties of nanosized materials can be related to the degree of interaction with the substrate. This phenomenon can be correlated to a downshift of the binding energy as it was put in evidence recently with platinum clusters onto oxide sites of an oxide–carbon composite.[1] Strong interactions between platinum clusters and highly oriented pyrolitic graphite (HOPG),[2] single-walled carbon nanotubes (SWNTs), multiwalled carbon nanotubes (MWNTs), and XC-72 carbon black substrates[3,4] have also been brought to light and recently explained by the possible formation of non-bonding π electronic states of graphite due to Pt–C hybridization.[5] This interaction seems responsible for lowering the adsorption energy of CO on platinum clusters and consequently leads to a weakening of the Pt–CO bond.[6] The strength of the interaction of metal nanoparticles with π sites on carbon supports provided resistance to metal sintering during heat treatment of the supported catalysts.[7] Metal substrate interactions can be actually studied by examining the adsorption behavior of carbon monoxide when used as a molecular probe. It was employed, e.g., on copper dispersed onto ruthenium.[8] In electrochemistry the use of this molecule in the process of the CO stripping to probe the electronic properties of well-oriented surfaces as well as materials in nanodivided form essentially based on Pt is commonplace[9−14] since the shape and the oxidation peaks of the adsorbed carbon monoxide reveal such interactions. Furthermore, it is well-known that CO is an intermediate of alcohol oxidation and the reforming of hydrocarbons processes. The CO produced from the oxidation of small organics plays a critical role in fuel cell applications because this molecule can strongly be adsorbed on the platinum electrode surface, thus blocking the catalytic sites and slowing the reaction kinetics.[15] Therefore, the design of anodic or cathodic catalysts able to weaken the adsorption of carbon monoxide is of special interest for fuel cell applications. In this connection, research was done to improve the activity of Pt-based catalysts toward the CO oxidation by focusing on the effect of their particle size[16−19] as well as by alloying Pt with 3d metals.[20−23] Additionally, it was shown that strong metal–substrate interaction (SMSI) can be obtained by selectively depositing platinum onto oxide sites of the carbon–oxide nanocomposites. This interaction is responsible for modifying the catalytic properties of Pt-based catalysts.[1,24−33] At this point it is not clear what the chemical ingredient is that switches the electronic changes of the catalytic site when it is in intimate contact with the substrate. It seems, however, logical that this switching mechanism must be in strong relationship with the chemical surface structure of the substrate that makes it possible for that the SMSI effect to be observed on other kinds of substrates. We report on new aspects of the interaction resulting from the functionalization between platinum nanoparticles and graphitic carbon-based substrates solely such as Vulcan XC-72, MWCNT, and graphene-like (HOPG surface) and TiO_2/carbon (with carbon = Vulcan XC-72 or MWCNT). The effects of graphitized carbon on Pt activity are so pronounced that they are even observable on TiO_2-supported Pt, where another strong metal–support interaction between Pt and TiO_2 is already in effect.[1,24−27] In this paper, we

Received: May 22, 2012
Revised: September 24, 2012
Published: September 24, 2012

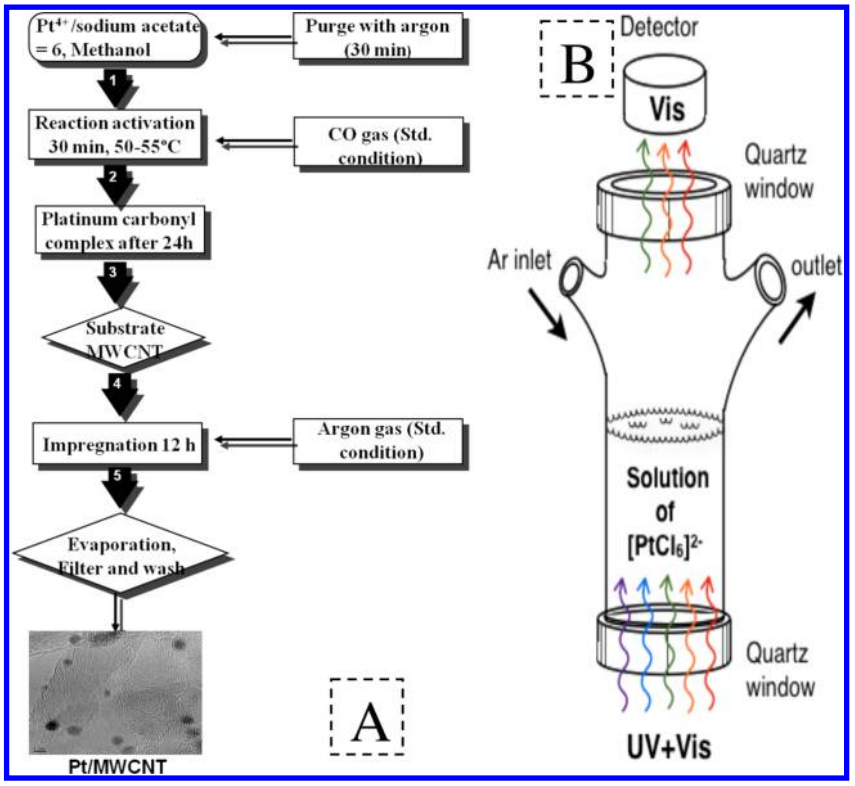

Figure 1. (A) Scheme of the carbonyl synthesis procedure. (B) Photoinduced deposition of platinum onto the oxide sites of oxide−carbon composites.

demonstrate for the first time that the magnitude of the promoting effect of carbon substrate on the catalytic activity of platinum clusters toward CO oxidation seems highly correlated with the in-plane crystallite size of carbon-based materials. This has been achieved by combining the results obtained from CO stripping and Raman spectroscopy experiments.

2. EXPERIMENTAL SECTION

2.1. Chemicals. We used $Na_2PtCl_6{\cdot}6H_2O$ and $H_2PtCl_6{\cdot}6H_2O$ from Alfa-Aesar, $TiCl_2$, $Na_2PtCl_6{\cdot}6H_2O$, and $H_2PtCl_6{\cdot}6H_2O$ from Alfa-Aesar, $TiCl_2$ and CH_3COONa from Sigma-Aldrich, methanol and tetrahydrofuran (THF) from Sigma-Aldrich, $Ti[OCH(CH_3)_2]_4$ and isopropanol from Sigma-Aldrich, MWCNT from Sigma-Aldrich, Vulcan XC-72 from Cabot, HOPG (highly oriented pyrolitic graphite) and glassy carbon (GC) from GoodFellow. MWCNT-m was synthesized by decomposing toluene inside fused silica tubing previously covered with a Fe-based organometallic compound thin film. Then MWCNT-m was treated with nitric acid in a reflux system at a temperature between 80 and 100 °C.[34]

2.2. Synthesis of Pt/MWCNT, Pt/C (Vulcan, HOPG, GC), and $Pt_{0.5}Ti_{0.5}$/C Catalysts via the Carbonyl Route. Pt−carbonyl complex was synthesized as usual by using methanol as a solvent through the reaction of Pt under CO at around 50−55 °C for 24 h with constant stirring until the color of the solution turned black green.[22,35] The molar ratio between sodium ions and hexachloroplatinic acid was fixed to 6. After synthesis of Pt−carbonyl complex, multiwalled carbon nanotubes (MWCNT, MWCNT-m) or Vulcan XC-72 (preannealed at 400 °C for 4 h under N_2) or HOPG or GC were added to the carbonyl complex solution under an inert gas atmosphere for 12 h in order to obtain the catalyst with 20 wt % loading onto the substrates. The powder was recovered after the solvent evaporation by rinsing with Milli-Q water (18.2 MΩ cm) to eliminate the impurities. The powder was recovered by filtration and then dried overnight. The entire procedure is schematized in Figure 1A. For the Pt−Ti synthesis, and due to the low solubility of $TiCl_2$ in methanol solvent, THF solvent was used. According to the desired stoichiometric quantities, the amount of $TiCl_2$ added was adjusted to a Ti^{2+}/Pt^{4+} ratio of 1. The molar ratio between sodium and hexachloroplatinic ions was fixed to 6. The mixture was reacted under CO at around 50−55 °C for 24 h with constant stirring until the color of solution turned dark. After synthesis of the $Pt_{0.5}Ti_{0.5}$−carbonyl complex, Vulcan XC-72 (preannealed at 400 °C for 4 h under N_2) was added to the solution under an inert gas atmosphere for 12 h in order to obtain the catalyst with 20 wt % loading onto the substrates.

2.3. Synthesis of Oxide−Carbon Composites (TiO_2/MWCNT, TiO_2/C) and Pt/TiO_2/MWCNT, Pt/TiO_2/C Supported Catalysts. The oxide−carbon composites TiO_2/MWCNT and TiO_2/C were prepared with 20 wt % loading of anatase nanoparticles which was prepared via the sol−gel method by mixing MWCNT and Vulcan XC-72 with titanium isopropoxide in isopropanol solvent.[24,25] In short, to prepare 20 wt % oxide−carbon composite, the carbon matrix was dispersed in isopropanol for 1 h by sonication. 185 μL of titanium isopropoxide was added into the suspension and mixed for another 1 h at 0 °C. 1 mL of Milli-Q water (18.2 MΩ cm at 0 °C) was added to hydrolyze TiO_2 nanoparticles, and the solution was stirred for 24 h. This process was conducted at 0 °C in order to slow the hydrolysis reaction kinetics and to improve the dispersion of the oxide onto the carbon matrix. The obtained powder was recovered by filtering, washing with Milli-Q water, and drying in vacuum overnight. The TiO_2/MWCNT and TiO_2/C composites were used as substrates for

dx.doi.org/10.1021/jp304947y | J. Phys. Chem. C 2012, 116, 21788−21794

depositing Pt nanoparticles. The required mass loading of platinum was 20 wt %. The deposition procedure was carried out as follows: oxide−carbon was mixed in argon-saturated water in a photoreactor provided with an optical quartz window. An isopropanol solution containing Pt salt ($H_2PtCl_6 \cdot 6H_2O$) was added into the photoreactor and stirred for 3 h under illumination via an ultraviolet (UV)-lamp (Xe lamp, 159 W). Visible and infrared light was filtered out by a hot mirror UV (Silica), while a water filter (long-pass filter GG400) was used to prevent heating of the samples. Figure 1B is a schematic representation of the experimental setup. The electron and hole pairs photogenerated via UV irradiation, onto oxide sites of the composite, reduced $[PtCl_6]^{2-}$ to Pt^0 via $[PtCl_4]^{2-}$ [24,25,36−38] and oxidized the isopropanol, respectively.

2.4. Physical Characterization. *Raman Spectroscopy.* A HORIBA Jobin Yvon Labram HR800UV Raman spectrometer provided with an Ar^+ laser (Melles Griot) as an illumination source equipped with a CCD cooled detector was used. The Raman instrument was coupled to an Olympus microscope provided with a 100× microscope objective. The laser frequency used was the 514.5 nm line. The laser power at the sample was of 0.04 mW. The spectra were recorded at 1 cm^{-1} resolution. Simulations were done by using Fityk software (free software).

Thermal Gravimetric Analysis/Differential Thermal Analysis (TG-DTA). TG-DTA measurements were carried out on a SDT Q600 thermal analyzer in air condition at a scan rate of 5 °C min^{-1} in the range from room temperature to 800 °C to obtain information on the decomposition and combustion properties of catalysts.

Electrochemical Measurements. The catalytic ink was prepared as follows: a mixture containing 10 mg of catalytic powder, 250 μL of Nafion solution (5 wt % in water/aliphatic alcohol solution, Sigma-Aldrich), and 1250 μL of Milli-Q water (18.2 MΩ cm) was sonicated for 30 min, and then an aliquot of 3 μL of the mixture was dropped onto the glassy carbon disk (GC) electrode (surface area of 0.071 cm^2) and dried in a stream of inert gas (argon) at room temperature for 20 min. The electrochemical measurements were carried out at 25 °C by using a potentiostat (Autolab PGSTAT 30) in a thermostated three-electrode one-compartment cell. The electrolyte was prepared with concentrated H_2SO_4 (Suprapur, Merck) and Milli-Q water (18.2 MΩ cm). A plate of glassy carbon (GC) and a reversible hydrogen electrode (RHE) were respectively used as counter and reference electrode. This latter electrode was placed into a Luggin capillary. For CO-stripping experiments, CO was bubbled into the electrolyte (0.5 M H_2SO_4) for 10 min, while the working electrode is biased at 0.1 V vs RHE. Then, dissolved CO was removed by bubbling nitrogen gas for 20 min. Two successive cyclic voltammograms were recorded from 0.05 to 1.2 V vs RHE with a scan rate of 5 mV s^{-1}. The current densities were normalized to the geometric surface area of the electrode.

3. RESULTS AND DISCUSSION

3.1. Physical Characterization. Results obtained in the spectral region of 1100−1800 cm^{-1} with Vulcan XC-72, MWCNT, MWCNT-m, and HOPG substrates are presented in Figure 2. It is evident that this spectral region shows several overlapping bands. The physical origin of each band is described in the Supporting Information. The parameters characterizing all Raman modes for each sample are summarized in Table 1. The D and D′ bands are defect-induced bands and are not visible in the HOPG sample (Figure 2). It is clear from this figure that the graphitic structures of both Vulcan XC-72 and MWCNT possess a high degree of interstitial disorder along the *c*-axis between the crystallite planes.[39] This can be deduced from the intensity of the band centered at ca. 1500 cm^{-1}, which actually reaches an amazing magnitude in these two samples. Additionally, these two carbonaceous materials contain more sp^3-rich phases than the other ones since the intensity of their 1200 cm^{-1} band is huge. In the case of the MWCNT sample, the presence of these two bands is a surprising feature although it was already reported for nanotubes made by chemical vapor deposition (CVD) process. This probably results from the presence of an amorphous carbon layer on the nanotubes external walls.

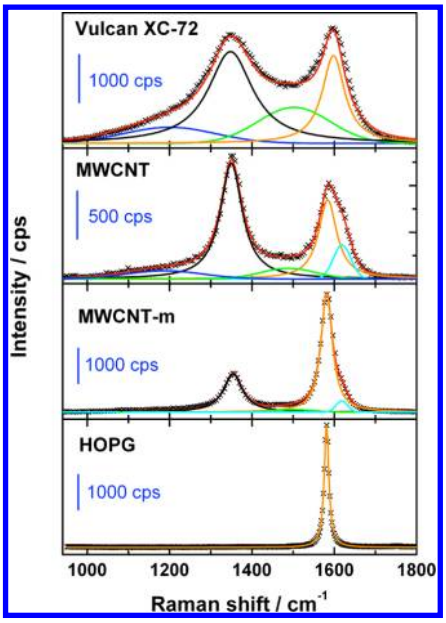

Figure 2. From top to bottom, the Raman spectra of Vulcan XC-72, MWCNT, MWCNT-m, and HOPG.

Table 1. Raman Parameters Obtained after Curve Fitting All the Investigated Samples[a]

	Vulcan XC-72	MWCNT	MWCNT-m	HOPG
υ_D (cm^{-1})	1350	1353	1354	N/A
$\omega_{1/2D}$ (cm^{-1})	131	65	56	N/A
υ_G (cm^{-1})	1598	1584	1582	1581
$\omega_{1/2G}$ (cm^{-1})	66	54	34	14
I_D/I_G	2.1	1.7	0.5	N/A
L_a (nm)	8	9.6	31.5	∞

[a] υ_D and υ_G respectively correspond to D and G bands positions. $\omega_{1/2D}$ and $\omega_{1/2G}$ respectively correspond to full width at half-maximum (FWHM) of D and G bands. L_a represents the in-plane crystallite size determined from eq 1.

The simulations of different spectra were performed. Lorentzian line shapes were used for D and G bands,[39−41] whereas Gaussian ones were used to simulate the D′ band[40,42] as well as the bands centered at ca. 1200 cm^{-1} [39,43] and 1500 cm^{-1}.[39] For the fitting, the positions of D and G bands were set by taking into account the second-order Raman spectrum and particularly the positions of 2D (ca. 2700 cm^{-1}) and D + G (ca. 2940 cm^{-1}) bands. The results of the best fits provided several parameters which are presented in Table 1. The I_D/I_G values correspond to integrated intensity ratios of D to G bands.

dx.doi.org/10.1021/jp304947y | J. Phys. Chem. C 2012, 116, 21788−21794

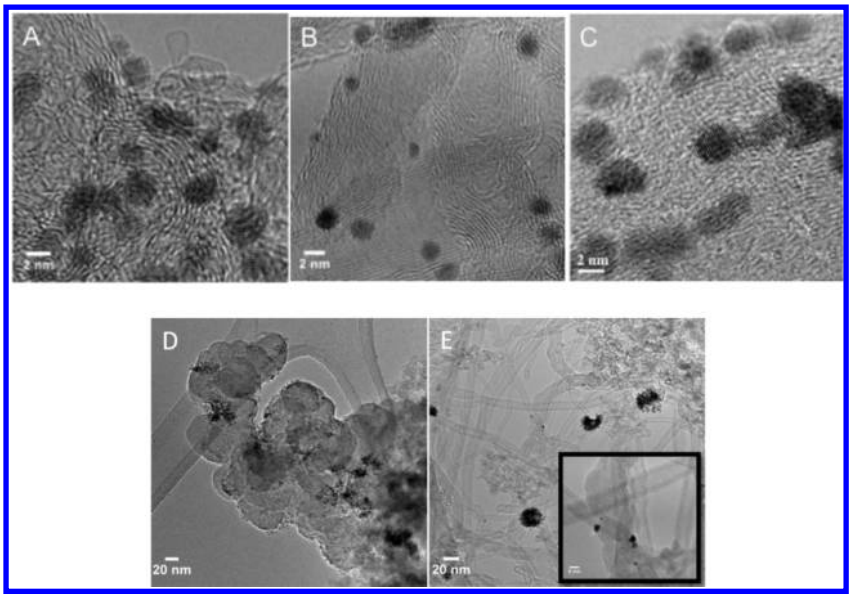

Figure 3. TEM images for (A) Pt/C, (B) Pt/MWCNT, (C) Pt/MWCNT-m, (D) Pt/TiO_2/C, and (E) Pt/TiO_2/MWCNT catalysts as-prepared.

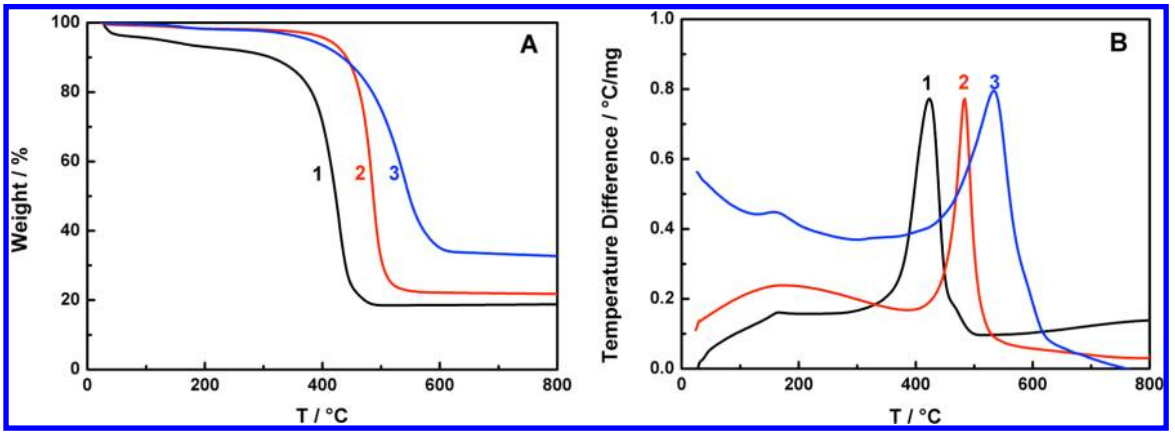

Figure 4. TG-DTA curves for (1) Pt/C, (2) Pt/MWCNT, and (3) Pt/MWCNT-m catalysts as-prepared.

Except for the G-band position of Vulcan XC-72, no significant shift, both for G and D-band positions, can be observed. The upward shift observed for G-band of Vulcan XC-72, located at 1598 cm^{-1}, probably results from the high degree of disorder of the corresponding sample. It is in fact well-known that the G band of disordered solids is shifted to higher Raman wavenumbers than the G band of ordered ones.[44] Additionally, this shift is responsible for nonseparation of G and D′ bands. As a result, the observed bands include both G and D′ ones. The magnitude of the shift is directly related to the percentage of contribution of D′.[45] The disordered character of both Vulcan XC-72 and MWCNT samples is in fair agreement with observed D and G line widths of these two samples. The decrease in both band widths is evidence for the increase of the ordering degree. The I_D/I_G ratio allows evaluation of the degree of graphitization of a carbonaceous material. This ratio is commonly used both to quantify the amount of defects in the carbon-based materials as well as the in-plane crystallite size (L_a). Consequently, it is also a measure of the interdefect distance. One of the relations describing the evolution of L_a with the integrated intensity ratio of G to D bands is the following one:[46]

$$L_a\ (\mathrm{nm}) = 2.4 \times 10^{-10} \lambda_{laser}{}^4 \frac{I_G}{I_D} \quad (1)$$

where λ_{laser} is the laser wavelength in nm.

From L_a values, calculated for all investigated samples, it can be deduced that both Vulcan XC-72 and MWCNT samples have a low crystallite size and do not possess extended graphitic domains. Additionally the width of the D-band of these two samples can reflect a broad distribution of in-plane crystallite size. Conversely, it can be deduced that, MWCNT-m possesses larger in-plane crystallites. For the HOPG sample, the in-plane crystallite size tends toward infinite.

Low-magnification images of Pt/C, Pt/MWCNT, and Pt/MWCNT-m catalysts are shown in parts A, B, and C of Figure 3, respectively. Platinum nanoparticles are well-dispersed on the carbon matrix in all cases, and the mean average particle size is of 1.9 ± 0.9, 2.1 ± 1.0, and 2.0 ± 1.0 nm, respectively. Particles photodeposited onto oxide-carbon composites are often agglomerated, and the agglomerates of some tens of nanometers are clearly visible. The photodeposition of Pt nanoparticles does not take place in the same way on the oxide−Vulcan XC-72 or oxide−MWCNT composites. It seems that the metal deposition is performed selectively onto the oxide surface when Vulcan XC-72 is used as carbon material (Figure 3D).

dx.doi.org/10.1021/jp304947y | J. Phys. Chem. C 2012, 116, 21788−21794

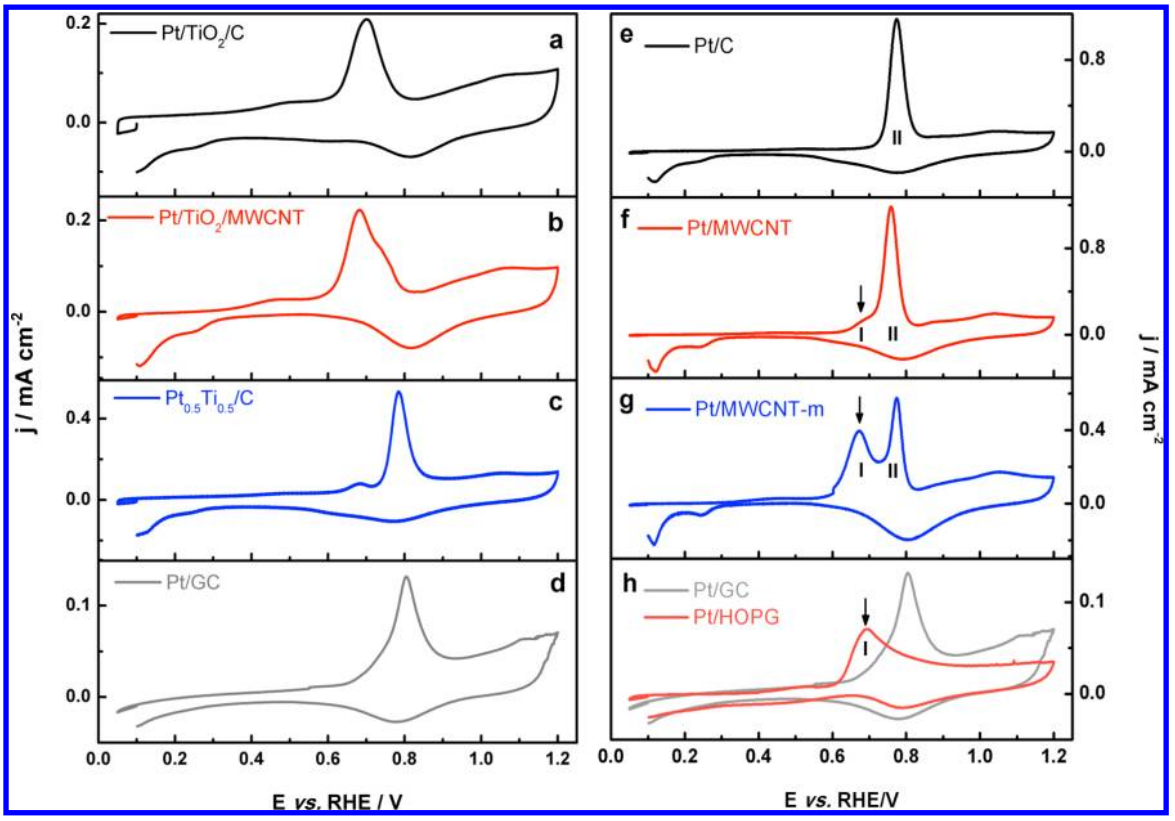

Figure 5. CO stripping in 0.5 M H_2SO_4 at 25 °C with 5 mV/s on catalysts for (a) $Pt/TiO_2/C$, (b) $Pt/TiO_2/MWCNT$, (c) $Pt_{0.5}Ti_{0.5}/C$, (d) Pt/GC, (e) Pt/C, (f) Pt/MWCNT, (g) Pt/MWCNT-m, and (h) Pt/HOPG and Pt/GC.

Surprisingly, in the case of oxide–MWCNT, Pt deposits onto both surfaces of oxide and MWCNT (Figure 3E); see e.g., the inset in Figure 3E. This effect is probably the result of the partial semiconducting behavior of MWCNT whose electron–hole pair separation could be responsible for reducing hexachloroplatinic ion and oxidizing isopropanol. The theoretical semiconducting energy of carbon nanotubes has been reported.[47]

TG-DTA thermal analysis done in air for Pt/carbon is shown in Figure 4. First, the TGA curves (Figure 4A) show that the dominant weight loss occurs from 400 to 600 °C. This is clearly related to the combustion of carbon. The carbon decomposition temperature of the Pt/C catalyst is 423 °C and increases up to 534 °C for the Pt/MWCNT-m catalyst. This increase in the decomposition temperature is in good agreement with the above-described Raman experiments. It is, in fact, well-known that the decomposition temperature of a carbon substrate increases with its degree of graphitization.

3.2. Electrochemical Characterization: CO Stripping. Figure 5 show special features concerning the CO-stripping voltammograms realized on various platinum-supported nanocatalysts. These characteristics clearly point out the different ways to obtain a CO-tolerant Pt catalyst by analyzing the platinum interaction with a reliable substrate. Substrates used in this study are either carbon-based materials (MWCNT, MWCNT-m, Vulcan XC-72, HOPG) or TiO_2/carbon (MWCNT, Vulcan XC-72) composites. The well-known strong metal–substrate interaction (SMSI) occurring between TiO_2 and platinum[24,25,48] is illustrated in Figure 5a,b. It can be clearly seen that this interaction leads to a main CO oxidation peak centered at 0.67 V vs RHE. A small oxidation peak appears at 0.68 V vs RHE (Figure 5c) on the Pt–Ti bimetallic as-prepared system that contains a low-alloyed fraction, as determined by XRD and STEM (data not shown).This result is evidence that the strong metal–substrate interaction between TiO_2 and Pt results in the formation of an alloyed material at the platinum–oxide interface which has a different electronic structure than pure platinum,[26] and which forms a weaker bond with CO molecules under electrochemical conditions. Moreover, the shape of the CO stripping voltammograms is affected by the chemical nature of the carbon material used to synthesize the TiO_2/carbon composite. This can be clearly inferred by comparing the CO stripping voltammogramms performed with $Pt/TiO_2/C$ catalyst (Figure 5a) and with Pt/TiO_2/MWCNT catalyst (Figure 5b). For $Pt/TiO_2/MWCNT$, the main CO oxidation peak is accompanied by a shoulder. This latter is centered at ca. 0.68 V vs RHE and corresponds to CO oxidation at platinum sites interacting with the oxide support. The second peak, centered at ca. 0.76 V vs RHE, can be associated with CO oxidation at platinum sites interacting with the graphitic carbon support. This correlation is greatly supported by TEM experiments which show that a part of photodeposited platinum directly interacts with graphitic carbon support (MWCNT).

Additionally, the classical interaction between platinum and Vulcan XC-72 leads to a CO oxidation peak located at 0.78 V vs RHE (Figure 5e). CO stripping voltammogramms realized with Pt/carbon (carbon = Vulcan XC-72, MWCNT, or MWCNT-m) electrocatalysts synthesized by the carbonyl way are shown in parts e, f, and g of Figure 5, respectively. The results contrasted in these figures, the main CO oxidation potential region (0.60 V vs RHE < E < 0.94 V vs RHE), can be explained by taking into account two different interaction sites between platinum and the carbon supports. The oxidation

dx.doi.org/10.1021/jp304947y | J. Phys. Chem. C 2012, 116, 21788–21794

region features two successive CO oxidation peaks. The first one (I) is located at ca. 0.67−0.68 V vs RHE and the second one (II) at ca. 0.76−0.77 V vs RHE. The comparison between the voltammogramms in Figure 5f,g with the one obtained in Figure 5h makes it clear that the first and second peak can be attributed to the CO oxidation at platinum sites interacting with graphitized and disordered carbon structures, respectively.

This finding is strongly supported by Raman experiments (see above). It seems that the ratio of the area (A_I) of peak I located at 0.67−0.68 V vs RHE to the total area ($A_T = A_I + A_{II}$) of peak I located at 0.67−0.68 V vs RHE, and peak II located at 0.76−0.77 V vs RHE, A_I/A_T, is clearly dependent on the graphitization degree of the carbon support. This data can be rationalized by correlating the oxidation of the probe molecule with the in-plane crystallite size, L_a, of the various carbons (see Table 2).

Table 2. Comparison of A_I/A_T Area Ratio (Extracted from CO Stripping Experiments) with the In-Plane Crystallite Size, L_a (Obtained from Raman Experiments), for the Different Investigated Carbon Supports

	A_I/A_T	L_a (nm)
Vulcan XC-72	0	8
MWCNT	0.13	9.6
MWCNT-m	0.60	31.5
HOPG	1	∞

From the data of Table 2, it is clear that the area ratio of peak I to the total peak increases when L_a increases, i.e., when the long-distance order increases in the graphitized structure. The potential shift observed for peak I is clearly associated with the interaction of platinum with long and well-ordered graphitized domains. Though this interaction is not entirely understood, some explanations can be given. It is possible that, as a result of the Pt−C interaction, a strong decrease in Pt−Pt bond distance takes place.[6] This can be favored during the heterogeneous nucleation and further growth of platinum particles onto the surface of the carbon support which may be responsible for the increase of the overlapping of d-orbitals by strongly increasing d−d interactions between platinum atoms as occurring in gold.[49] As a result of the contraction phenomenon, a d-band movement, away from the Fermi level, is possible. Consequently, the interaction between the adsorbate states and metal valence band states can be strongly modified leading to changes in the interaction energy.[50,51] Additionally, the adsorption phenomenon of CO at the platinum surface is accompanied by back-donation of platinum d-orbital into the unoccupied $2\pi^*$-orbital of CO. As a result of such interaction, between platinum and well-ordered graphitized domains, it is possible that the charge transfer occurs from Pt to C (according to the respective electronegativities of the elements) leading to a decrease in the d-orbital back-donation and consequently to a weakening of the Pt−CO bond. Further experiments will be carried out using X-ray photoelectron spectroscopy as well as in-situ FTIR experiments to try to clarify this issue.

4. CONCLUSIONS

In this work, we have investigated the substrates effect using the carbon monoxide as a molecular probe. Different ways of modifying the catalytic behavior of platinum toward CO oxidation are presented and discussed. Pt/TiO_2/carbon (Vulcan XC-72, MWCNT) catalysts were synthesized by the photodeposition method. Based on the study of their electrocatalytic activity toward CO oxidation and TEM characterization, a strong metal−support interaction effect of of platinum nanoparticles on graphitized carbon was observed similar to that of platinum onto TiO_2−carbon composite substrates. In this latter one, it has been demonstrated that the origin of their catalytic activity modification results from the formation of a Pt−Ti interfacial alloy structure. Interestingly, a similar negative shift of adsorbed CO electro-oxidation was obtained on catalysts by functionalizing the Pt onto graphitic carbon (MWCNT, MWCNT-m, HOPG graphene-like) by the carbonyl chemical route. From Raman experiments it can be deduced that this negative shift is likely related to the degree of graphitization of the considered carbon substrate and consequently to its in-plane crystallite size. This new interaction feature clearly shows that intimate and strong interaction between platinum and carbon can take place. However, to better understand this interaction, more investigations are needed.

■ ASSOCIATED CONTENT

Supporting Information

Raman bands description. This material is available free of charge via the Internet at http://pubs.acs.org.

■ AUTHOR INFORMATION

Corresponding Author

*E-mail: nicolas.alonso.vante@univ-poitiers.fr.

Notes

The authors declare no competing financial interest.

■ ACKNOWLEDGMENTS

J. Ma thanks the fellowship of the Poitou-Charentes region for financial support. The authors acknowledge Dr. Y. Verde, Technological Institute of Cancún, Mexico, for the MWCNT-m samples kindly provided.

■ REFERENCES

(1) Lewera, A.; Timperman, L.; Roguska, A.; Alonso-Vante, N. *J. Phys. Chem. C* **2011**, *115*, 20153−20159.
(2) Yang, D. Q.; Zhang, G. X.; Sacher, E.; José-Yacamán, M.; Elizondo, N. *J. Phys. Chem. B* **2006**, *110*, 8348−8356.
(3) Wu, G.; Chen, Y.-S.; Xu, B.-Q. *Electrochem. Commun.* **2005**, *7*, 1237−1243.
(4) Torre, T.; Aricò, A. S.; Alderucci, V.; Antonucci, V.; Giordano, N. *Appl. Catal., A* **1994**, *114*, 257−272.
(5) Kondo, T.; Iwasaki, Y.; Honma, Y.; Takagi, Y.; Okada, S.; Nakamura, J. *Phys. Rev. B* **2009**, *80*, 233408.
(6) Oh, J.; Kondo, T.; Hatake, D.; Iwasaki, Y.; Honma, Y.; Suda, Y.; Sekiba, D.; Kudo, H.; Nakamura, J. *J. Phys. Chem. Lett.* **2009**, *1*, 463−466.
(7) Coloma, F.; Sepulvedaescribano, A.; Rodriguezreinoso, F. *J. Catal.* **1995**, *154*, 299−305.
(8) Hoffmann, F. M.; Paul, J. *J. Chem. Phys.* **1987**, *87*, 1857−1865.
(9) Gasteiger, H. A.; Markovic, N.; Ross, P. N.; Cairns, E. J. *J. Phys. Chem.* **1994**, *98*, 617−625.
(10) Koper, M. T. M.; Lukkien, J. J.; Jansen, A. P. J.; van Santen, R. A. *J. Phys. Chem. B* **1999**, *103*, 5522−5529.
(11) Green, C. L.; Kucernak, A. *J. Phys. Chem. B* **2002**, *106*, 11446−11456.
(12) Koper, M. T. M.; Lebedeva, N. P.; Hermse, C. G. M. *Faraday Discuss.* **2002**, *121*, 301−311.
(13) Maillard, F.; Savinova, E. R.; Simonov, P. A.; Zaikovskii, V. I.; Stimming, U. *J. Phys. Chem. B* **2004**, *108*, 17893−17904.

(14) Urchaga, P.; Baranton, S.; Coutanceau, C.; Jerkiewicz, G. *Langmuir* **2011**, *28*, 3658−3663.
(15) Arenz, M.; Mayrhofer, K. J. J.; Stamenkovic, V.; Blizanac, B. B.; Tomoyuki, T.; Ross, P. N.; Markovic, N. M. *J. Am. Chem. Soc.* **2005**, *127*, 6819−6829.
(16) Savinova, E. R.; Hahn, F.; Alonso-Vante, N. *Surf. Sci.* **2009**, *603*, 1892−1899.
(17) Friedrich, K. A.; Henglein, F.; Stimming, U.; Unkauf, W. *Electrochim. Acta* **2000**, *45*, 3283−3293.
(18) Mukerjee, S.; McBreen, J. *J. Electroanal. Chem.* **1998**, *448*, 163−171.
(19) Min, M.-k.; Cho, J.; Cho, K.; Kim, H. *Electrochim. Acta* **2000**, *45*, 4211−4217.
(20) Wang, J.; Holt-Hindle, P.; MacDonald, D.; Thomas, D. F.; Chen, A. *Electrochim. Acta* **2008**, *53*, 6944−6952.
(21) Beard, B. C.; Ross, P. N. *J. Electrochem. Soc.* **1990**, *137*, 3368−3374.
(22) Yang, H.; Alonso-Vante, N.; Léger, J. M.; Lamy, C. *J. Phys. Chem. B* **2004**, *108*, 1938−1947.
(23) Waszczuk, P.; Solla-Gullón, J.; Kim, H. S.; Tong, Y. Y.; Montiel, V.; Aldaz, A.; Wieckowski, A. *J. Catal.* **2001**, *203*, 1−6.
(24) Timperman, L.; Alonso-Vante, N. *Electrocatalysis* **2011**, *2*, 181−191.
(25) Timperman, L.; Feng, Y. J.; Vogel, W.; Alonso-Vante, N. *Electrochim. Acta* **2010**, *55*, 7558−7563.
(26) Timperman, L.; Lewera, A.; Vogel, W.; Alonso-Vante, N. *Electrochem. Commun.* **2010**, *12*, 1772−1775.
(27) Vogel, W.; Timperman, L.; Alonso-Vante, N. *Appl. Catal., A* **2010**, *377*, 167−173.
(28) Tacconi, N. R. d.; Rajeshwar, K.; Chanmanee, W.; Valluri, V.; Wampler, W. A.; Lin, W.-Y.; Nikiel, L. *J. Electrochem. Soc.* **2010**, *157*, B147−B153.
(29) De Tacconi, N. R.; Chenthamarakshan, C. R.; Rajeshwar, K.; Lin, W. Y.; Carlson, T. F.; Nikiel, L.; Wampler, W. A.; Sambandam, S.; Ramani, V. *J. Electrochem. Soc.* **2008**, *155*, B1102−B1109.
(30) Somasundaram, S.; Chenthamarakshan, C. R.; de Tacconi, N. R.; Basit, N. A.; Rajeshwar, K. *Electrochem. Commun.* **2006**, *8*, 539−543.
(31) Ghosh, T.; Vukmirovic, M. B.; DiSalvo, F. J.; Adzic, R. R. *J. Am. Chem. Soc.* **2009**, *132*, 906−907.
(32) Sasaki, K.; Zhang, L.; Adzic, R. R. *Phys. Chem. Chem. Phys.* **2008**, *10*, 159−167.
(33) Sasaki, K.; Adzic, R. R. *J. Electrochem. Soc.* **2008**, *155*, B180−B186.
(34) Antúnez-Flores, W.; Valenzuela-Muñiz, A. M.; Amézaga-Madrid, P.; Alonso-Nuñez, G.; Verde, Y.; Martínez-Sánchez, R.; Miki-Yoshida, M. *J. Nanosci. Nanotechnol.* **2008**, *8*, 6451−6455.
(35) Favry, E.; Wang, D.; Fantauzzi, D.; Anton, J.; Su, D. S.; Jacob, T.; Alonso-Vante, N. *Phys. Chem. Chem. Phys.* **2011**, *13*, 9201−9208.
(36) Sugimura, H.; Uchida, T.; Kitamura, N.; Masuhara, H. *Chem. Lett.* **1993**, *2*, 379−382.
(37) Juodkazis, S.; Ishii, H.; Matsuo, S.; Misawa, H. *J. Electroanal. Chem.* **1999**, *473*, 235−239.
(38) Harada, M.; Einaga, H. *Langmuir* **2006**, *22*, 2371−2377.
(39) Jawhari, T.; Roid, A.; Casado, J. *Carbon* **1995**, *33*, 1561−1565.
(40) Antunes, E. F.; Lobo, A. O.; Corat, E. J.; Trava-Airoldi, V. J.; Martin, A. A.; Veríssimo, C. *Carbon* **2006**, *44*, 2202−2211.
(41) Castillejos, E.; Bachiller-Baeza, B.; Pérez-Cadenas, M.; Gallegos-Suarez, E.; Rodríguez-Ramos, I.; Guerrero-Ruiz, A.; Tamargo-Martinez, K.; Martinez-Alonso, A.; Tascón, J. M. D. *J. Alloys Compd.* **2012**, *536* (Suppl. 1), S460−S463.
(42) Mennella, V.; Monaco, G.; Colangeli, L.; Bussoletti, E. *Carbon* **1995**, *33*, 115−121.
(43) Tang, X. M.; Weber, J.; Mikhailov, S. N.; Müller, C.; Hänni, W.; Hintermann, H. E. *J. Non-Cryst. Solids* **1995**, *185*, 145−150.
(44) Cuesta, A.; Dhamelincourt, P.; Laureyns, J.; Martínez-Alonso, A.; Tascón, J. M. D. *Carbon* **1994**, *32*, 1523−1532.
(45) Vidano, R.; Fischbach, D. B. *J. Am. Ceram. Soc.* **1978**, *61*, 13−17.
(46) Cancado, L. G.; Takai, K.; Enoki, T.; Endo, M.; Kim, Y. A.; Mizusaki, H.; Jorio, A.; Coelho, L. N.; Magalhaes-Paniago, R.; Pimenta, M. A. *Appl. Phys. Lett.* **2006**, *88*, 163106.
(47) Ando, T. *NPG Asia Mater* **2009**, *1*, 17−21.
(48) Vogel, W.; Timperman, L.; Alonso-Vante, N. *Appl. Catal., A* **2010**, *377*, 167−173.
(49) Visikovskiy, A.; Matsumoto, H.; Mitsuhara, K.; Nakada, T.; Akita, T.; Kido, Y. *Phys. Rev. B* **2011**, *83*, 165428.
(50) Hammer, B.; Nørskov, J. K. *Surf. Sci.* **1995**, *343*, 211−220.
(51) Mavrikakis, M.; Hammer, B.; Nørskov, J. K. *Phys. Rev. Lett.* **1998**, *81*, 2819−2822.